Nuclear Engineering and Technology 54 (2022) 3833–3840

Contents lists available at ScienceDirect

Nuclear Engineering and Technology

journal homepage: www.elsevier.com/locate/net

Original Article

Development of an energy and efficiency calibration method for stilbene scintillators

Chanho Kim [a, b], Jaehyo Kim [c], Wooseong Hong [c], Jung-Yeol Yeom [a, b, d, e, *], Geehyun Kim [c, f, g, **]

[a] Department of Bio-Convergence Engineering, Korea University, Seoul, South Korea
[b] Department of Bioengineering, Korea University, Seoul, South Korea
[c] Department of Energy Systems Engineering, Seoul National University, Seoul, South Korea
[d] School of Biomedical Engineering, Korea University, Seoul, South Korea
[e] Interdisciplinary Program in Precision Public Health, Korea University, Seoul, South Korea
[f] Department of Nuclear Engineering, Seoul National University, Seoul, South Korea
[g] Institute of Engineering Research, Seoul National University, Seoul, South Korea

ARTICLE INFO

Article history:
Received 8 March 2022
Received in revised form
27 May 2022
Accepted 16 June 2022
Available online 20 June 2022

Keywords:
Stilbene scintillator
Organic scintillator
Energy calibration
Intrinsic detection efficiency
Compton scattering
Klein–Nishina formula

ABSTRACT

A method for calibrating the energy scale and detection efficiency of stilbene scintillators is presented herein. This method can be used to quantitatively analyze the Compton continuum of gamma-ray spectra obtained using such scintillators. First, channel–energy calibration was conducted by fitting a semi-empirical equation for the Compton continuum to the acquired energy spectrum and a new method to evaluate the intrinsic detection efficiency, called intrinsic Compton efficiency, of stilbene scintillators was proposed. The validity of this method was verified by changing experimental conditions such as the number of sources being measured simultaneously and the detector–source distance. According to the energy calibration, the standard error for the estimated Compton edge position was ±1.56 keV. The comparison of the intrinsic Compton efficiencies calculated from the single- and two-source spectra showed that the mean absolute difference and the mean absolute percentage difference are 0.031 %p and 0.557%, respectively, demonstrating reasonable accuracy of this method. The feasibility of the method was confirmed for an energy range of 0.5–1.5 MeV, showing that stilbene scintillators can be used to quantitatively analyze gamma rays in mixed-radiation fields.

1. Introduction

Scintillators play an important role as radiation detection materials in various nuclear technologies and radiation applications, such as nuclear medicine, border control, and nuclear decommissioning [1,2]. They are generally classified as organic and inorganic scintillators, and the scintillator type used in a radiation detector is selected according to the radiation particles to be measured and the purpose of radiation detection. Organic scintillators are widely used in applications such as high-energy physics, environmental radiation monitoring, and nuclear security because of their relatively short decay time, low material cost, and ability to be easily manufactured in large sizes and various shapes [3,4]. In particular, some organic scintillators, such as stilbene and liquid scintillators, have excellent pulse-shape discrimination (PSD) capabilities to distinguish neutrons from gamma rays while having high sensitivity to both. Therefore, organic scintillators are preferred for applications related to nuclear activity detection and nuclear security verification based on the detection of neutrons and gamma rays emitted from radioactive materials. However, because they comprise low-atomic-number elements, organic scintillators have limited capability in gamma-ray detection; in particular, the full-energy peak (photopeak) does not appear in the measured energy spectrum.

In gamma-ray spectroscopy, a photopeak in the energy spectrum represents the original energy of the gamma rays incident on the detector. This photopeak is often well localized and can be

* Corresponding author. Department of Bio-Convergence Engineering, Korea University, Seoul, South Korea.
** Corresponding author. Department of Energy Systems Engineering, Seoul National University, Seoul, South Korea.
E-mail addresses: manngo@korea.ac.kr (C. Kim), jungyeol@korea.ac.kr (J.-Y. Yeom), gk.rs@snu.ac.kr (G. Kim).

https://doi.org/10.1016/j.net.2022.06.016

Abbreviations

ADC	Analog-to-digital converter
BR	Branching ratio
CE	Compton edge
CM	Compton maximum
CoP	An integrated charge of pulse
PSD	Pulse shape discrimination
ROI	Region of interest

easily analyzed without much complication. Therefore, the photopeak is used to obtain information regarding the radiation detector, such as its peak-detection efficiency, and calibrate its energy scale. However, owing to the low-atomic-number elements in organic scintillators, the most dominant reaction between organic scintillators and gamma rays is Compton scattering. Hence, the photopeak is barely visible in the energy spectrum. Therefore, it is difficult to calibrate the energy scale of organic scintillators and determine their gamma-ray detection efficiency to obtain radioactivity information of the gamma-ray source. These disadvantages in gamma spectroscopy limit the sole use of organic scintillators in the applications requiring concurrent detection of neutrons and gamma rays.

In general, the dual detection of gamma rays and neutrons is often performed by combining two single-particle detectors. However, a dual-particle imaging system, which simultaneously detects gamma rays and neutrons, has advantages over the single-particle imaging systems because it allows the identification of a variety of nuclear materials and is more suitable for locating them in complex environments [5]. Elpasolite scintillators such as Cs_2LiYCl_6:Ce, Tl_2LiYCl_6:Ce, and $Cs_2LiLaCl_6$:Ce can provide good gamma-ray energy resolution while detecting neutrons [6,7]. However, these scintillators mainly detect thermal neutrons and normally have low sensitivity for fast neutrons [8], making it difficult to obtain the original neutron source location and the energy information of the incident neutrons. Meanwhile, organic scintillators can detect fast neutrons, providing information of the source location and the energy of the incident neutrons. Therefore, if we could quantitatively analyze incident gamma rays by measuring them with organic scintillators, these devices could be versatilely used for the simultaneous detection of neutrons and gamma rays.

Before using an organic scintillator for gamma-ray spectroscopy, its energy calibration should be performed. A common calibration method for this purpose relies on the identification of the Compton edge (CE) position. That is, the exact position of the CE in the Compton continuum should be first determined to properly calibrate the energy-dependent response of the organic scintillator. This can be done, for example, by estimating the CE position based on the data fitting between the spectra obtained via Monte Carlo simulation and energy spectrum [9–11]. For the energy calibration of organic scintillators, other researchers have used coincidence techniques by detecting scattered photons using a reference gamma-ray detector in addition to an organic scintillator [12,13]. They successfully calibrated the energy scale of the organic scintillators and identified the exact CE position. Nevertheless, the quantitative analysis of the gamma-ray spectra obtained using organic scintillators still has considerable complications, e.g., unlike the Gaussian-shaped photopeak, the CE region in the Compton continuum, by nature, presents asymmetric features. This makes it difficult to determine the gamma-ray detection efficiency of these detectors that provide a consistent way to quantify incident gamma rays associated with the activity of a specific gamma-ray source.

In the present study, we attempted to determine the CE position by fitting semiempirical equations for describing the Compton continuum regarding the gamma-ray spectra obtained using a stilbene scintillator, which is a widely used scintillator type for fast neutron detection owing to its excellent PSD performance compared with other organic scintillators [14,15]. Furthermore, we propose a region-of-interest (ROI) that can be used as an index to represent the nuclide-specific radiation response instead of a photopeak, which is barely visible in the gamma-ray spectra obtained using a stilbene scintillator. The proposed method does not require an additional reference radiation detector to apply the Compton coincidence technique and numerous Monte Carlo simulation results to fit the data. Our study aimed to resolve the energies of the incident gamma rays and determine the detection efficiency of the stilbene scintillators, which aid in estimating the activity of the gamma-ray source. We repeated the measurement experiments using different gamma-ray sources to calibrate the detector's energy scale and calculated the intrinsic detection efficiency of the stilbene scintillator.

2. Materials and methods

2.1. Gamma-ray spectrum measurements

A 5.08-cm-diameter stilbene scintillator (Inrad Optics, Northvale, NJ, USA) coupled to a 5.1-cm-diameter Hamamatsu R6231-100 photomultiplier tube (PMT) was used for detecting the gamma rays. The PMT was supplied with a voltage of 1000 V, and its anode signal was directly sent to a high-speed DT5730 digitizer (500 MS/s, 14-bit resolution, CAEN). The digitized signal obtained by measuring ^{137}Cs (344.00 ± 8.02 kBq), ^{22}Na (119.25 ± 2.78 kBq), and ^{60}Co (220.90 ± 5.15 kBq) check sources was used to obtain the gamma-ray spectra. We varied the distance between the source and detector (20, 25, and 30 cm). After independent measurements of each source, simultaneous measurements of two sources (^{137}Cs and ^{22}Na or ^{137}Cs and ^{60}Co) were conducted. Each measurement was conducted for 20 min. Finally, the background gamma-ray spectrum was obtained through a 2-h measurement and subtracted from each gamma-ray spectrum for spectral analysis.

The detector signal processing system was implemented by entirely digitizing each pulse using the DT5730 digitizer without performing any amplification or shaping procedure. The sampling rate of each pulse was 500 MHz, and the interval between each sampling point was 2 ns. The digitized channel values obtained using the analog-to-digital converter (ADC) corresponded to the time-series current values of the PMT output signal, which is directly related to the number of scintillation photons arriving at PMT in real time. Therefore, the amount of energy deposited by an incident gamma ray corresponded to the sum of the ADC channel values converted from each sampling point of the PMT output signal pulse. The duration for the summation of the ADC channel values was set from the front point to the endpoint of each pulse, providing 1% amplitude of the pulse peak before and after reaching the peak in the signal pulse. The sum of the ADC channel values of each pulse is often referred to as an integrated charge of pulse (CoP, expressed in arbitrary unit [arb. unit]) [16,17].

2.2. Calculation of the compton continuum

Because a stilbene scintillator comprises low-atomic-number elements, Compton scattering is the dominant interaction for gamma rays with an energy > 0.1 MeV. The energy distribution of the Compton recoil electrons, i.e., the Compton continuum, can be derived using the Klein–Nishina formula and expressed as follows

[10,18]:

$$\frac{d\sigma_c}{dT}=\frac{\pi r_e^2}{m_e c^2\gamma^2}\left[2+\frac{s^2}{\gamma^2(1-s)^2}+\frac{s}{1-s}\left(s-\frac{2}{\gamma}\right)\right], \quad (1)$$

where T indicates the energy of the scattered electron, σ_c denotes the Compton scattering cross section, r_e represents the classical electron radius, $\gamma = h\nu/m_e c^2$, and $s = T/h\nu$. The energy distribution can be blurred by the contribution of electronic noise and statistical fluctuations in the light generation and collection mechanism, which can be approximated as a Gaussian distribution. Then, the distribution of the energy deposited by Compton recoil electrons can be expressed by convoluting Equation 1 with the Gaussian distribution as follows:

$$Compton\left({}^{A}X\right)=C\int_0^{E_{max}}\frac{d\sigma_c}{dT}\frac{1}{\sqrt{2\pi}\sigma}e^{-\frac{b(E-T)}{2\sigma^2}}dT, \quad (2)$$

where $Compton({}^{A}X_E)$ represents the Compton continuum resulting from gamma-ray photons having energy E emitted from a nuclide ${}^{A}X$, E_{max} denotes the maximum energy of the Compton recoil electrons, corresponding to the CE, σ represents the standard deviation of Gaussian distribution, b denotes an energy scaling parameter to provide the CoP value associated with the CE, and C denotes a normalization constant to conform the number of gamma rays detected using the detector. The Compton maximum (CM), which has the highest count in the Compton continuum of energy spectrum, can be easily observed in the obtained energy spectrum and $Compton({}^{A}X_E)$; thus, parameter C is determined first. Subsequently, the fitting procedure was performed by adjusting σ, and b until obtaining the smallest root mean square error between the calculated $Compton({}^{A}X_E)$ and the obtained energy spectrum.

For gamma-ray sources emitting multiple energies, such as ^{60}Co and ^{22}Na, the total Compton continuum can be obtained by linearly combining the contributions from each energy using branching ratios. For example, in the case of a ^{60}Co source, the total Compton continuum can be expressed as

$$Compton\left({}^{60}Co_{Total}\right)=BR_1\times Compton\left({}^{60}Co_{1173\ keV}\right)+BR_2\times Compton\left({}^{60}Co_{1332\ keV}\right), \quad (3)$$

where BR_1 and BR_2 represent the branching ratios for gamma-ray photons of 1173 and 1332 keV emitted from ^{60}Co, respectively. Conversely, the contributions from each energy can be separated by subtracting each Compton continuum component from the combined spectrum. Thus, we applied Equation 3 to the energy spectra of ^{22}Na and ^{60}Co, obtaining the individual contributions of ${}^{22}Na_{511\ keV}$, ${}^{22}Na_{1274\ keV}$, ${}^{60}Co_{1173\ keV}$, and ${}^{60}Co_{1332\ keV}$.

2.3. Energy calibration

The response of an organic scintillator will be dependent on the type of the incident particle depositing its energy to the scintillator. The response of the scintillator to electrons is linear for the energy > 125 keV [19]. Therefore, the energy response of the organic scintillator can be calibrated as per incident gamma rays and fast electrons. The relationship between CoP and the energy deposited by the recoil electron T can be expressed as

$$CoP = pT + q, \quad (4)$$

where p is a parameter used to match the CoP values with the energy values and q is a parameter called the offset charge, which is required owing to the nonlinear of the scintillator response to electrons at low electron energies (<125 keV). q is sufficiently smaller compared with the typical energy [20]. To calibrate the energy scale of a stilbene detector used in this study, we performed the energy calibration through linear regression between CoP values and CE using Equation 4. For the energy calibration, we used gamma rays with the energies of 662, 511, 1274, 1173, and 1332 keV, and the corresponding CE values were 340.67, 477.33, 963.42, 1061.70, and 1118.10 keV, respectively.

2.4. Detection efficiency

To quantitatively evaluate the energy-dependent gamma-ray detection efficiency of a stilbene scintillator, we defined a new efficiency parameter to represent the distal response of Compton continuum associated with the incident gamma-ray energy, called intrinsic Compton efficiency ($\varepsilon_{int.C}$).

Based on the fundamental definition of intrinsic detection efficiency [19], $\varepsilon_{int.C}$ was calculated in the Compton region as follows:

$$\varepsilon_{int.C}=\frac{Counts\ of\ ROI\ in\ Compton\ continuum\ area\ (N_{comp})}{number\ of\ radiation\ photons\ incident\ on\ detector\ (N_{int})} \quad (5)$$

with

$$N_{int}=number\ of\ radiation\ photons\ emitted\ from\ source\ (N_t)\times\frac{\Omega}{4\pi}$$

and

$$N_t = Activity\ (\text{in Bq})\times BR\times Time\ (\text{in s}),$$

where $Time$ is the measurement time and N_{comp} denotes the number of events in the ROI of the energy spectrum. The ROI must

Table 1
Average intrinsic Compton efficiency ($\varepsilon_{int.C}$) values, mean absolute differences, and mean absolute percentage differences for various regions-of-interests (ROIs).

Index	ROI range		Average [a] $\varepsilon_{int.C}$	Mean absolute difference	Mean absolute percentage difference
	Min	Max			
ROI-1	[b] $E_{CE}-(FWHM/2)$	$E_{CE}+(FWHM/2)$	3.32% ± 0.08%	0.019%p	0.581%
ROI-2	[c] $E_{CM}-(FWHM/2)$	$E_{CM}+(FWHM/2)$	4.13% ± 0.10%	0.038%p	0.906%
ROI-3	$E_{CM}-(FWHM/2)$	$E_{CE}+(FWHM/2)$	5.10% ± 0.12%	0.031%p	0.557%
ROI-4	$E_{CE}-(FWTM/2)$	$E_{CE}+(FWTM/2)$	5.43% ± 0.13%	0.037%p	0.645%
ROI-5	$E_{CM}-(FWTM/2)$	$E_{CM}+(FWTM/2)$	6.63% ± 0.15%	0.095%p	1.334%
ROI-6	$E_{CM}-(FWTM/2)$	$E_{CE}+(FWTM/2)$	7.06% ± 0.16%	0.196%p	2.494%

[a] Average value for five gamma-ray energies (511, 662, 1173, 1274, and 1332 keV).
[b] Energy of CE in Compton continuum.
[c] Energy of CM in Compton continuum.

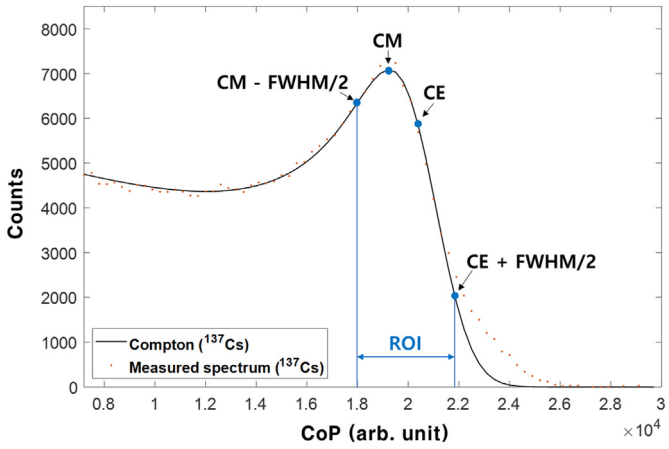

Fig. 1. Energy spectrum of ^{137}Cs and corresponding Compton continuum (*Compton(^{137}Cs)*) with the region-of-interest (ROI).

be carefully selected as a region that can be used as an index to represent the nuclide-specific radiation response instead of the photopeak, which barely exists in the gamma-ray energy spectra measured using an organic scintillator. Furthermore, the ROI is used for the gamma-ray detection efficiency calibration of the organic scintillator.

To verify the feasibility of our method, we observed the consistency of the $\varepsilon_{int.C}$ values by comparing the $\varepsilon_{int.C}$ values obtained via different experimental setups. First, we calculated and compared the $\varepsilon_{int.C}$ values resulting from single-source measurement spectra (^{137}Cs, ^{22}Na, and ^{60}Co) and two-source measurement spectra (simultaneously measuring i) ^{137}Cs and ^{22}Na and ii) ^{137}Cs and ^{60}Co). Furthermore, we calculated the $\varepsilon_{int.C}$ values while changing the source–detector distance and observed the consistency of $\varepsilon_{int.C}$ values.

Before calculating the $\varepsilon_{int.C}$ values, the ROI should be carefully selected. We considered both the magnitude and consistency of $\varepsilon_{int.C}$ to set an ROI that can serve as a large enough and consistent index for determining the $\varepsilon_{int.C}$. Accordingly, we determined the ROI

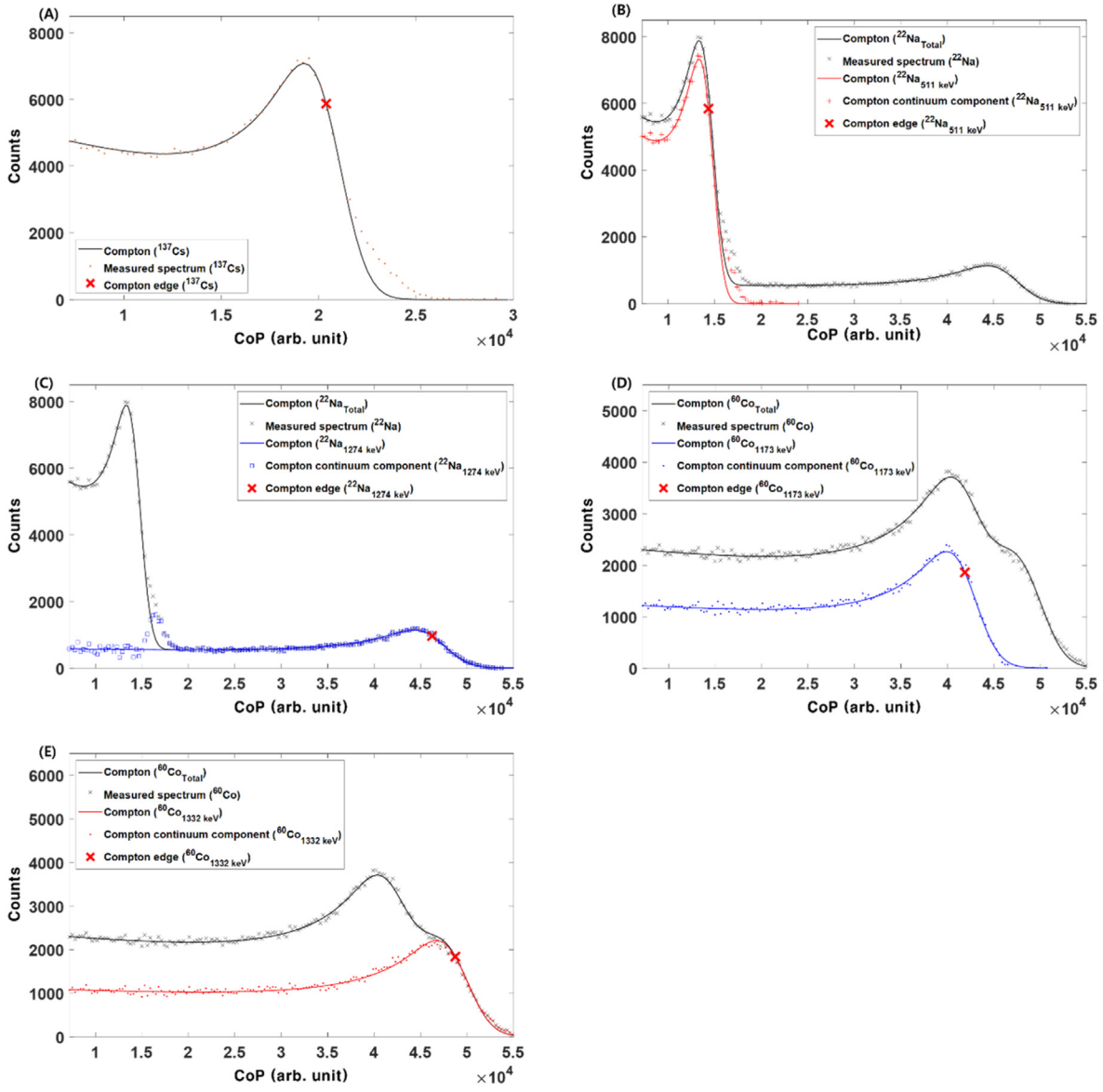

Fig. 2. Energy spectra and corresponding Compton continua (*Compton($^{A}X_E$)*) for (A) ^{137}Cs, (B) ^{22}Na$_{511\ keV}$, (C) ^{22}Na$_{1274\ keV}$, (D) ^{60}Co$_{1173\ keV}$, and (E) ^{60}Co$_{1332\ keV}$.

by comparing the mean absolute percentage difference between the $\varepsilon_{int.C}$ values derived from the energy spectra of single- and two-source measurements. To reduce the effect of electrical noise and low-energy background, we tested the CE, which has the highest energy in the Compton continuum, as the ROI centroid. Moreover, we considered the CM as one of the ROI centroids because it was located on high energy region in the Compton continuum and can be easily found in the spectrum. We tested various types of ROI ranges defined in terms of full width at half maximum (FWHM) and full width at tenth maximum (FWTM), which were derived from the σ value used in Equation 2 to consider the response uncertainty to the deposited energy. Table 1 summarizes the resulting average $\varepsilon_{int.C}$ values, mean absolute differences, and mean absolute percentage differences for various ROIs. The mean absolute difference is the average of absolute differences of the $\varepsilon_{int.C}$ values derived from the energy spectra of single- and two-source measurements for five gamma-ray energies. The mean absolute percentage difference is the average of the percentage values obtained by dividing the absolute $\varepsilon_{int.C}$ difference by the $\varepsilon_{int.C}$ value obtained from a single-source measurement. As shown in Table 1, although ROI-1 provided the smallest mean absolute difference, ROI-3 could achieve the smallest mean absolute percentage difference because of its relatively high efficiency. Therefore, in our experiment, the ROI range was determined as follows:

$$ROI = \left[E_{CM} - \left(\frac{FWHM}{2}\right),\ E_{CE} + \left(\frac{FWHM}{2}\right)\right] \tag{6}$$

$$FWHM = 2\sqrt{2ln2}\sigma$$

$$FWTM = 2\sqrt{2ln10}\sigma,$$

where σ, the same parameter as in Equation 2, determines the FWHM of the Gaussian distribution through its relation with the standard deviation. Fig. 1 shows the ^{137}Cs gamma-ray energy spectrum obtained with the ROI determined using Equation 6.

In gamma-ray spectroscopy, the energy resolution of a detector is typically considered as a key parameter to represent its capability to resolve different energies of incident quanta. Therefore, it is conventionally defined as the FWHM of the photopeak divided by the location of the peak centroid. Furthermore, it is conceptually comparable to "impulse response" such as point spread function in signal processing. Several studies on the energy response of organic scintillators based on the Compton continuum [9,10] have mixedly used the term "energy resolution" as a criterion to evaluate the characteristics of the scintillator by defining it in terms of the FWHM of the Compton continuum area around the CE. However, by considering the fundamental definition and concept of energy resolution, we presume that the terminology referring to the continuum response should be distinguished from the terminology referring to the response to the full-energy deposition (impulse). In this regard, the expression of "energy resolution" for discussing the response of the (Compton) continuum needs to be used more carefully because the continuum responses do not really "resolve" any specific (or peak) instance or event caused by incident radiation quanta. In this study, we propose to discuss the characteristics of the continuum response obtained using an organic scintillator in terms of the response uncertainty or FWHM rather than the energy resolution.

Table 2
Energy and charge of pulse (CoP) values corresponding to the Compton edges.

Radionuclide	Energy	Compton edge	CoP (arb. unit)
^{137}Cs	662 keV	477 keV	20,486 ± 286
^{22}Na	511 keV	341 keV	14,314 ± 239
	1274 keV	1062 keV	46,362 ± 431
^{60}Co	1173 keV	963 keV	41,888 ± 409
	1332 keV	1118 keV	48,825 ± 442

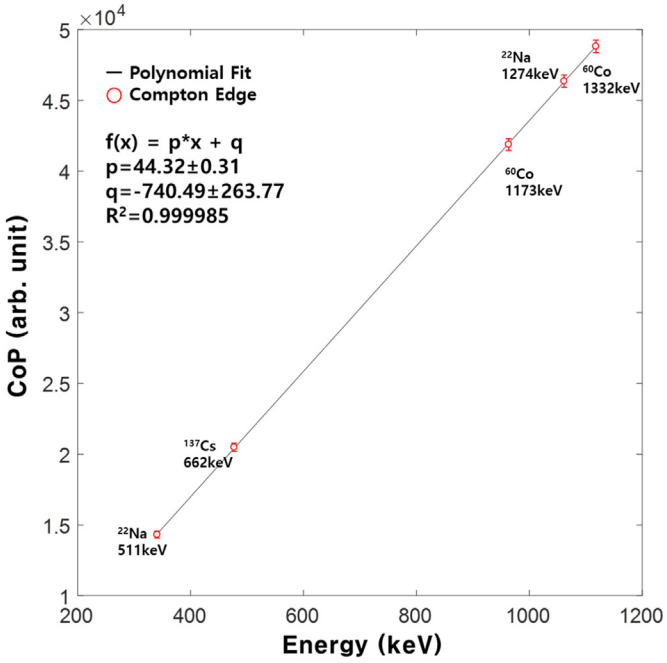

Fig. 3. Energy calibration curve of the stilbene scintillator obtained using five Compton edge positions; the error bars represent 95% confidence intervals (±2σ).

3. Results and discussion

3.1. Energy calibration

The CoP values (corresponding to CE) obtained from the energy spectra of the gamma rays having different energies (Fig. 2) are presented in Table 2. The reported CoP values were determined via the fitting procedure. Linear regression was performed to obtain the linear relation between the gamma-ray energy and CoP of the associated pulse. The slope and intercept of the linear fitting plot were 44.32 ± 0.31 arb. unit per keV and −740.49 ± 263.77 arb. unit, respectively, as illustrated in Fig. 3. In this study, the ratio of the CE count to CM count is 82.9 % in the Cs-137 energy spectrum, and it is similar to other studies [14,21] that used 80% CE to CM ratio to determine the CE position using the stilbene scintillator. In principle, the ratio between the CE and CM count cannot be constant and may vary depending on the energy of incident gamma rays. The position (energy) of CE is determined according to the gamma-ray energy, while the position (energy) of CM, in nature, depends on the response uncertainty (i.e., σ in Equation 2) of the detector related to the gamma-ray energy. If an ideal detector is considered, the position of CM will coincide with that of CE. However, in a real detector that has a finite response uncertainty, the position of CM will shift to lower values than it of CE with an increase in response

Table 3
Intrinsic Compton efficiency ($\varepsilon_{int.C}$) values for the single-source measurements.

Radionuclide	Compton edge	FWHM	N_{comp}	$\varepsilon_{int.C}$
^{137}Cs	477 keV	61.93 keV	75,228 ± 549	5.83% ± 0.14%
^{22}Na	341 keV	52.04 keV	66,051 ± 514	6.98% ± 0.17%
	1062 keV	109.03 keV	22,091 ± 297	4.20% ± 0.11%
^{60}Co	963 keV	104.32 keV	42,066 ± 410	4.32% ± 0.11%
	1118 keV	109.26 keV	40,807 ± 404	4.19% ± 0.11%

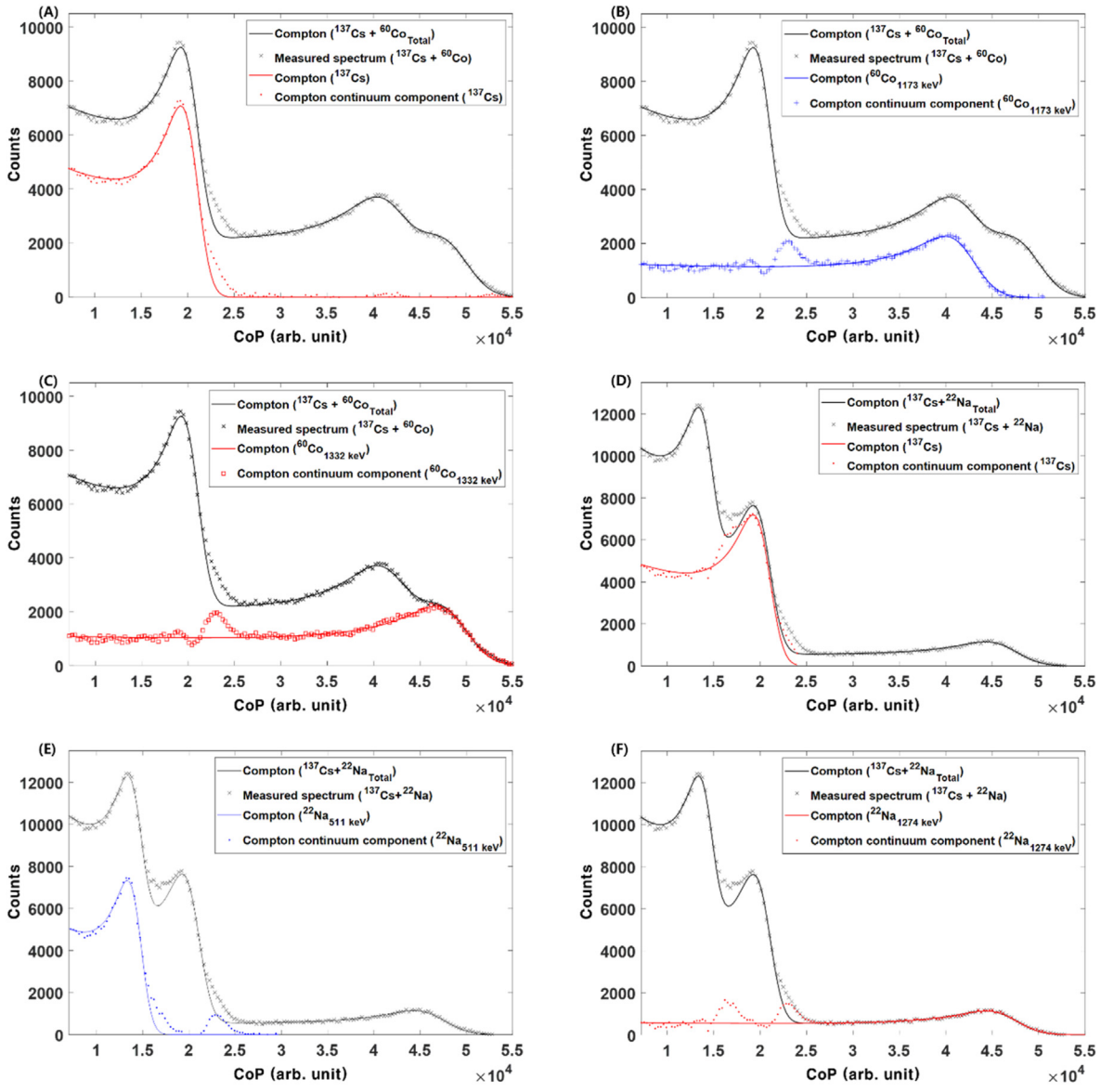

Fig. 4. Energy spectra obtained via two-source measurements and the corresponding Compton continua (*Compton*($^A X_E$)) for (A) ^{137}Cs, (B) ^{60}Co$_{1173\ keV}$, and (C)^{60}Co$_{1332\ keV}$ extracted from ^{137} Cs and ^{60}Co energy spectrum and (D) ^{137}Cs, (E)^{22}Na$_{511\ keV}$, and (F) ^{22}Na$_{1274\ keV}$ extracted from ^{137} Cs and ^{22}Na energy spectrum.

uncertainty. Therefore, the position of CM is energy dependent considering the relationship [19,22] between the response uncertainty of the detector, σ, and the gamma-ray energy.

According to the energy calibration, the discrepancy between the CE energy calculated from the linear regression using the reported CoP value, the original CE energy was ± 0.99, ±1.61, ±1.59, ±1.09, and ±0.26 keV at 340.67, 477.33, 963.42, 1061.70, and 1118.10 keV, respectively. The average discrepancy between five gamma-ray energies was ±1.11 keV, which demonstrates a reasonable accuracy of the proposed method for the energy calibration.

3.2. Intrinsic Compton efficiency

Table 3 summarizes the $\varepsilon_{int.C}$ values derived from the energy spectra shown in Fig. 2 by applying the ROI (i.e., ROI-3) described above. Notably, the $\varepsilon_{int.C}$ for the 662-keV gamma rays emitted from ^{137}Cs can be derived straightforwardly from the energy spectrum (Fig. 2A) because ^{137}Cs is a monoenergetic source. Thus, the Compton continuum associated with the incident gamma rays can be resolved without much ambiguity. Further, the FWHM can be calculated based on the σ value determined using the fitting procedure. Meanwhile, the sources emitting multiple gamma rays with different energies, i.e., ^{22}Na and ^{60}Co in our case, require additional steps to resolve each Compton continuum component from the combined spectrum. Compton continuum components were obtained using Equation 3 and have been shown in Fig. 2. Moreover, the FWHMs and ROIs must be determined for each component, and the $\varepsilon_{int.C}$ values are calculated accordingly. In our experiment, the $\varepsilon_{int.C}$ values calculated for the incident gamma-ray energies of 511, 662, 1173, 1274, and 1332 keV were 6.98%, 5.83%, 4.32%, 4.20%, and 4.19%, respectively.

To verify the consistency of the calculated $\varepsilon_{int.C}$ values, we compared the $\varepsilon_{int.C}$ values derived from the energy spectra obtained via single- and two-source measurements. Fig. 4 displays the $\varepsilon_{int.C}$ values resulting from two-source measurements. Because the energy spectrum comprised several Compton continuum components corresponding to gamma rays with different energies, these

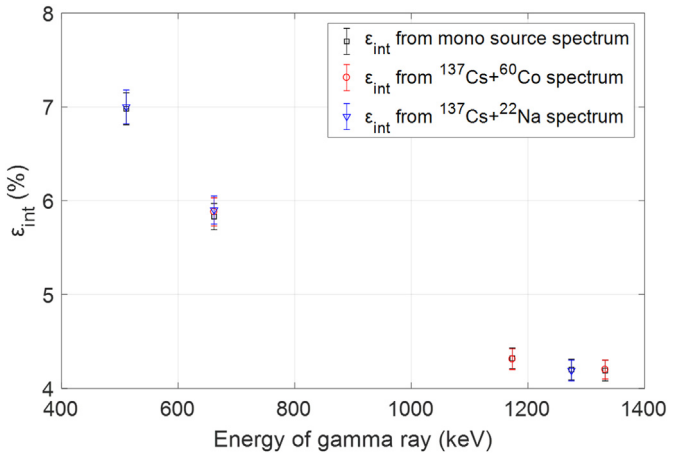

Fig. 5. Intrinsic Compton efficiencies ($\varepsilon_{int.C}$) derived from the energy spectra obtained via single- and two-source measurements; the error bars represent 95% confidence intervals ($\pm 2\sigma$).

Table 4
Intrinsic Compton efficiency ($\varepsilon_{int.C}$) values derived from the energy spectra obtained via single- and two-source measurements.

Radionuclide	Compton edge	Single-source	^{137}Cs +^{60}Co	^{137}Cs +^{22}Na
		$\varepsilon_{int.C}$	$\varepsilon_{int.C}$	$\varepsilon_{int.C}$
^{137}Cs	477.33 keV	5.83% ± 0.14%	5.88% ± 0.15%	5.90% ± 0.15%
^{22}Na	340.67 keV	6.98% ± 0.17%	-	7.00% ± 0.18%
	1061.70 keV	4.20% ± 0.11%	-	4.19% ± 0.11%
^{60}Co	963.42 keV	4.32% ± 0.11%	4.31% ± 0.11%	-
	1118.10 keV	4.19% ± 0.11%	4.20% ± 0.10%	-

components were extracted from the combined energy spectrum using Equation 3 (Fig. 4). *Compton($^{A}X_{E}$)* only considers the case of single Compton scattering; thus, some peaks that cause by multiple scattering exist in the Compton continuum component resolved from the combined spectrum. Fig. 5 and Table 4 compare the $\varepsilon_{int.C}$ values obtained through single- and two-source measurements, showing good agreement and consistency. The comparison confirmed that the mean absolute difference and mean absolute percentage difference were 0.031%p and 0.557%, respectively. This suggests that the proposed method can be used to calculate the

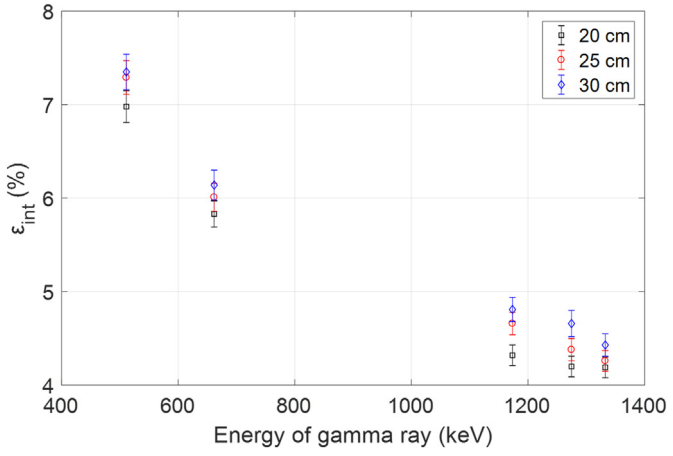

Fig. 6. Intrinsic Compton efficiencies ($\varepsilon_{int.C}$) derived from the energy spectra measured at various detector–source distances; the error bars represent 95% confidence intervals ($\pm 2\sigma$).

Table 5
Intrinsic Compton efficiencies ($\varepsilon_{int.C}$) derived from the energy spectra measured at various detector–source distances.

Radionuclide	Compton edge	$\varepsilon_{int.C}$ at different distance		
		20 cm	25 cm	30 cm
^{137}Cs	*477.33 keV*	*5.83% ± 0.14%*	*6.01% ± 0.15%*	*6.14% ± 0.16%*
^{22}Na	*340.67 keV*	*6.98% ± 0.17%*	*7.29% ± 0.18%*	*7.35% ± 0.19%*
	1061.70 keV	*4.20% ± 0.11%*	*4.38% ± 0.12%*	*4.66% ± 0.14%*
^{60}Co	*963.42 keV*	*4.32% ± 0.11%*	*4.66% ± 0.12%*	*4.81% ± 0.13%*
	1118.10 keV	*4.19% ± 0.11%*	*4.26% ± 0.11%*	*4.43% ± 0.12%*

efficiency consistently for the gamma rays in mono- and mixed-radiation fields. Meanwhile, because 1173- and 1332-keV gamma rays emitted from ^{60}Co and 1274-keV gamma rays emitted from ^{22}Na have a small energy difference compared with the response uncertainty to respective gamma-ray energies, the gamma rays from ^{60}Co and ^{22}Na were considered to be difficult to resolve. Therefore, the energy difference of gamma rays and FWHMs of detector response should be considered to resolve gamma rays using the proposed method.

Finally, we calculated the $\varepsilon_{int.C}$ values for different detector–source distances, and the results are shown in Fig. 6 and Table 5. The $\varepsilon_{int.C}$ value increased with increasing distance. This is expected to happen when the ratio between the detector radius and the source-to-detector distance is > 0.01 [23,24]. This is caused by the difference in the gamma-ray incidence angle on the detector. When the ratio between detector radius and distance is sufficiently small (<0.01), a consistent detection efficiency is expected for the gamma rays of specific energy.

4. Conclusion

Herein, we developed a novel calibration method that derives the CE position from the gamma-ray spectra obtained using stilbene scintillators and quantitatively analyzes these energy spectra. A fitting procedure was performed between the experimental spectrum and the calculated *Compton($^{A}X_{E}$)*. Then, energy calibration was performed, and the intrinsic Compton efficiency was calculated to estimate the activity of the gamma-ray source. The proposed method can determine the exact CE position in the gamma-ray spectrum without conducting a Monte Carlo simulation or using reference detector. Furthermore, using this method, we successfully characterized the detection efficiency for each gamma-ray energy in a mixed-radiation field of up to three gamma rays with different energies. This method is applicable to stilbene and other organic scintillators in the absence of photopeaks and can quantify the intensity of incident gamma rays emitted from specific radioactive sources. This method can, thus, be applied to gamma-ray/neutron dual-particle imagers [25–28] using organic scintillators, which are extensively studied for border control, nuclear security, and nuclear decommissioning. The method's feasibility has been confirmed for the energy range of 0.5–1.5 MeV, and it can be used to quantitatively analyze gamma rays with fidelity in mono- and mixed-radiation fields using stilbene scintillators and possibly other organic scintillators by adjusting the fitting parameters.

CRediT authorship contribution statement

Chanho Kim: Conceptualization, Methodology, Investigation, Software, Writing - Original Draft. **Jaehyo Kim:** Software, Resources. **Wooseong Hong:** Software, Visualization, Resources. **Jung-Yeol Yeom:** Methodology, Writing - Review & Editing, Supervision. **Geehyun Kim:** Conceptualization, Writing - Review & Editing, Project administration, Funding acquisition.

Declaration of competing interest

The authors declare that they have no known competing financial interests or personal relationships that could have appeared to influence the work reported in this paper.

Acknowledgments

This work was supported by National Research Foundation of Korea (NRF) (2017M2A8A4017932, NRF-2018R1D1A1A02048400, and NRF-2020R1A2C2007376), and Korea Environmental Industry & Technology Institute (KEITI) through Subsurface Environment Management (SEM) Project, funded by Korea Ministry of Environment (MOE) (2018002440004).

References

[1] M.J. Cieślak, K.A.A. Gamage, R. Glover, Critical review of scintillating crystals for neutron detection, Crystals 9 (2019) 480.
[2] A. Osovizky, D. Ginzburg, A. Manor, R. Seif, M. Ghelman, I. Cohen-Zada, M. Ellenbogen, V. Bronfenmakher, V. Pushkarsky, E. Gonen, SENTIRAD—an innovative personal radiation detector based on a scintillation detector and a silicon photomultiplier, Nucl. Instruments Methods Phys. Res. Sect. A Accel. Spectrometers, Detect. Assoc. Equip. 652 (2011) 41–44.
[3] J. Nattress, I. Jovanovic, Response and calibration of organic scintillators for gamma-ray spectroscopy up to 15-MeV range, Nucl. Instruments Methods Phys. Res. Sect. A Accel. Spectrometers, Detect. Assoc. Equip. 871 (2017) 1–7, https://doi.org/10.1016/j.nima.2017.07.024.
[4] X. Wen, T. Harvey, R. Weinmann-Smith, J. Walker, Y. Noh, R. Farley, A. Enqvist, Characterization of a tin-loaded liquid scintillator for gamma spectroscopy and neutron detection, Nucl. Instruments Methods Phys. Res. Sect. A Accel. Spectrometers, Detect. Assoc. Equip. 897 (2018) 47–53, https://doi.org/10.1016/j.nima.2018.04.054.
[5] H. Al Hamrashdi, S.D. Monk, D. Cheneler, Passive gamma-ray and neutron imaging systems for national security and nuclear non-proliferation in controlled and uncontrolled detection areas: review of past and current status, Sensors (Basel) 19 (2019), https://doi.org/10.3390/s19112638.
[6] H.S. Kim, M.B. Smith, M.R. Koslowsky, S.-W. Kwak, S.-J. Ye, G. Kim, Characterization of a CLYC detector and validation of the Monte Carlo simulation by measurement experiments, J. Radiat. Prot. Res. 42 (2017) 48–55.
[7] H.S. Kim, S.-J. Ye, G. Lee, G. Kim, Optimization of the collimator mask for the rotational modulation collimator-based gamma-ray/neutron dual-particle imager, Curr. Appl. Phys. 19 (2019) 856–865.
[8] M.B. Smith, T. Achtzehn, H.R. Andrews, E.T.H. Clifford, P. Forget, J. Glodo, R. Hawrami, H. Ing, P. O'Dougherty, K.S. Shah, U. Shirwadkar, L. Soundara-Pandian, J. Tower, Fast neutron measurements using Cs2LiYCl6:Ce (CLYC) scintillator, Nucl. Instruments Methods Phys. Res. Sect. A Accel. Spectrometers, Detect. Assoc. Equip. 784 (2015) 162–167, https://doi.org/10.1016/j.nima.2014.09.021.
[9] S. Ashrafi, M. Ghahremani Gol, Energy calibration of thin plastic scintillators using Compton scattered gamma-rays, Nucl. Instruments Methods Phys. Res. Sect. A Accel. Spectrometers, Detect. Assoc. Equip. 642 (2011) 70–74, https://doi.org/10.1016/j.nima.2011.04.003.
[10] N. Kudomi, Energy calibration of plastic scintillators for low energy electrons by using Compton scatterings of gamma rays, Nucl. Instruments Methods Phys. Res. Sect. A Accel. Spectrometers, Detect. Assoc. Equip. 430 (1999) 96–99, https://doi.org/10.1016/S0168-9002(99)00200-4.
[11] E.R. Siciliano, J.H. Ely, R.T. Kouzes, J.E. Schweppe, D.M. Strachan, S.T. Yokuda, Energy calibration of gamma spectra in plastic scintillators using Compton kinematics, Nucl. Instruments Methods Phys. Res. Sect. A Accel. Spectrometers, Detect. Assoc. Equip. 594 (2008) 232–243, https://doi.org/10.1016/j.nima.2008.06.031.
[12] J.M. Régis, G. Pascovici, J. Jolie, M. Rudigier, The mirror symmetric centroid difference method for picosecond lifetime measurements via γ-γ coincidences using very fast LaBr3(Ce) scintillator detectors, Nucl. Instruments Methods Phys. Res. Sect. A Accel. Spectrometers, Detect. Assoc. Equip. 622 (2010) 83–92, https://doi.org/10.1016/j.nima.2010.07.047.
[13] L. Swiderski, M. Moszyński, W. Czarnacki, J. Iwanowska, A. Syntfeld-Każuch, T. Szczęśniak, G. Pausch, C. Plettner, K. Roemer, Measurement of Compton edge position in low-Z scintillators, Radiat. Meas. 45 (2010) 605–607, https://doi.org/10.1016/j.radmeas.2009.10.015.
[14] C. Kim, J.-Y. Yeom, G. Kim, Digital n-γ pulse shape discrimination in organic scintillators with a high-speed digitizer, J. Radiat. Prot. Res. 44 (2019) 53–63, https://doi.org/10.14407/jrpr.2019.44.2.53.
[15] M.L. Ruch, M. Flaska, S.A. Pozzi, Pulse shape discrimination performance of stilbene coupled to low-noise silicon photomultipliers, Nucl. Instruments Methods Phys. Res. Sect. A Accel. Spectrometers, Detect. Assoc. Equip. 793 (2015) 1–5.
[16] G. Dietze, H. Klein, Gamma-calibration of NE 213 scintillation counters, Nucl. Instruments Methods Phys. Res. 193 (1982) 549–556.
[17] T.A. Laplace, B.L. Goldblum, J.A. Brown, J.J. Manfredi, Scintillator light yield measurements with waveform digitizers, Nucl. Instruments Methods Phys. Res. Sect. A Accel. Spectrometers, Detect. Assoc. Equip. 959 (2020), 163485.
[18] W.R. Leo, Radiation protection. Biological effects of radiation, in: Tech. Nucl. Part. Phys. Exp., Springer, 1994, pp. 69–79.
[19] G.F. Knoll, Radiation Detection and Measurement, John Wiley & Sons, 2010.
[20] G. Dietze, IEEE Transaction on Nuclear Science, vol. 26, 1979, p. 398. NS-.
[21] M.M. Bourne, S.D. Clarke, N. Adamowicz, S.A. Pozzi, N. Zaitseva, L. Carman, Neutron detection in a high-gamma field using solution-grown stilbene, Nucl. Instruments Methods Phys. Res. Sect. A Accel. Spectrometers, Detect. Assoc. Equip. 806 (2016) 348–355.
[22] E.I. Prosper, O.J. Abebe, U.J. Ogri, Characterisation of cerium-doped lanthanum bromide scintillation detector, Lat. Am. J. Phys. Educ. 6 (2012) 162.
[23] A. Jehouani, R. Ichaoui, M. Boulkheir, Study of the NaI (Tl) efficiency by Monte Carlo method, Appl. Radiat. Isot. 53 (2000) 887–891.
[24] F.O. Ogundare, E.O. Oniya, F.A. Balogun, Dependence of NaI (Tl) detector intrinsic efficiency on source-detector distance, energy and off-axis distance: their implications for radioactivity measurements, Pramana 70 (2008) 863–874.
[25] J. Boo, M.D. Hammig, M. Jeong, Compact lightweight imager of both gamma rays and neutrons based on a pixelated stilbene scintillator coupled to a silicon photomultiplier array, Sci. Rep. 11 (2021) 1–14.
[26] W. Steinberger, N. Giha, M. Hua, S. Clarke, S. Pozzi, Anisotropic neutron response of trans-stilbene and impact on a handheld dual particle imager, Nucl. Instruments Methods Phys. Res. Sect. A Accel. Spectrometers, Detect. Assoc. Equip. 1003 (2021), 165266.
[27] H.S. Kim, J. Lee, S. Choi, Y. Bang, S.-J. Ye, G. Kim, Design and fabrication of CLYC-based rotational modulation collimator (RMC) system for gamma-ray/neutron dual-particle imager, J. Radiat. Prot. Res. 46 (2021) 112–119.
[28] H.S. Kim, G. Kim, S.-J. Ye, Dual-particle imaging performance of a Cs2LiYCl6:Ce (CLYC)-based rotational modulation collimator (RMC) system, IEEE Trans. Nucl. Sci. 69 (6) (2021) 1389–1396, https://doi.org/10.1109/TNS.2021.3140035.